Mechanical properties of small structures built by selective laser melting 316 L stainless steel – a phenomenological approach to improve component design

Mechanische Eigenschaften von kleinen Strukturen aus selektiv lasergeschmolzenem 316 L Edelstahl – ein phänomenologischer Ansatz zur Verbesserung des Bauteildesigns

L. Wiesent[1, 2], U. Schultheiß[3], P. Lulla[4], A. Nonn[1], U. Noster[3]

Experimental investigations are conducted to quantify the influence of specimen thickness and orientation on the mechanical properties of selective laser melted stainless steel 316 L. The results indicate that the mechanical strength and ductility increase with increasing specimen thickness until a saturation value is reached from a specimen thickness of about 2 mm. Specimen orientation dependency is pronounced for thin specimens (<1.5 mm), whereas only small deviations in strength are observed for thicker specimens with orientations of 30°, 45° and 90° to build direction. The mechanical properties of the specimen orientation of 0° to build direction shows great deviation to the other orientations and the smallest overall strength. A reliable design of selective laser melted components should account for specimen thickness and orientation, e.g. by a correction factor. Furthermore, it is recommended to avoid loads vertical (90°) and parallel (0°) to build direction to guarantee higher ductility and strength.

Keywords: 316 L / selective laser melting / mechanical characterization / size effect / additive manufacturing design recommendation

Anhand von experimentellen Untersuchungen wird der Einfluss der Probendicke und -orientierung auf die mechanischen Eigenschaften von selektiv lasergeschmolzenem Edelstahl 316 L ermittelt. Die Ergebnisse zeigen, dass die mechanische Festigkeit und Duktilität mit zunehmender Probendicke ansteigt bis ein Sättigungswert ab einer Probendicke von etwa 2 mm erreicht wird. Die Abhängigkeit

[1] Ostbayerische Technische Hochschule (OTH) Regensburg, Technologie Campus Neustadt a. d. Donau, Computational Mechanics and Materials Lab, Galgenbergstraße 30, 93053, REGENSBURG, FEDERAL REPUBLIC OF GERMANY
[2] OTH Regensburg, Regensburg Center of Biomedical Engineering (RCBE), Am Biopark 9, 93053, REGENSBURG, FEDERAL REPUBLIC OF GERMANY
[3] Ostbayerische Technische Hochschule (OTH) Regensburg, Material Sciences and Surface Analytics Lab, Galgenbergstraße 30, 93053, REGENSBURG, FEDERAL REPUBLIC OF GERMANY
[4] FIT Production GmbH, Am Grohberg 1, 92331, LUPBURG, FEDERAL REPUBLIC OF GERMANY

Corresponding author: L. Wiesent, Ostbayerische Technische Hochschule (OTH) Regensburg, Technologie Campus Neustadt a. d. Donau, Computational Mechanics and Materials Lab, Galgenbergstraße 30, 93053, REGENSBURG, FEDERAL REPUBLIC OF GERMANY,
E-Mail: lisa.wiesent@oth-regensburg.de

der mechanischen Eigenschaften von der Probenorientierung ist bei dünnen Proben (< 1.5 mm) stark ausgeprägt, während bei dickeren Proben mit Orientierungen von 30°, 45° und 90° zur Baurichtung nur geringe Abweichungen in der Festigkeit beobachtet werden. Die mechanischen Eigenschaften der Probenorientierung von 0° zur Baurichtung zeigt große Abweichungen zu den anderen Orientierungen, sowie die geringste Festigkeit. Eine zuverlässige Auslegung von selektiv lasergeschmolzenen Bauteilen sollte die Probendicke und -orientierung z. B. durch einen Korrekturfaktor berücksichtigen. Außerdem sollten Belastungen senkrecht (90°) und parallel (0°) zur Baurichtung vermieden werden, um eine höhere Duktilität und Festigkeit zu gewährleisten.

Schlüsselwörter: Selektives Laserschmelzen / mechanische Charakterisierung / Größeneinfluss / Designempfehlungen für die additive Fertigung

1 Introduction

Additive manufacturing has become increasingly popular during the last decades [1]. It is characterized by a layer-by-layer production in contrast to conventional subtractive manufacturing techniques. Additive manufacturing has many advantages, including low material consumption, enhanced design capabilities and high cost-effectiveness of small parts with complex geometry that makes it particularly suitable for lightweight, medical and customized applications [2]. Material properties of additive manufactured parts are strongly dependent on a variety of variables, including process parameters and component geometry [3–5]. To date, the resulting additive manufactured material properties, especially for filigree structures, are still insufficiently known. Although some guidelines for the design of additive manufactured components exist, most of them focus on geometric constraints regarding printability of bulk components (e. g. surface and dimension accuracy, wall thickness, supported or unsupported overhangs etc.) [6–9]. Guidelines concerning smaller additively manufactured structures, however, hardly exist which makes an adequate component design difficult, especially for filigree structures of additive manufactured components.

Selective laser melting of metal components is a powder bed based additive manufacturing process. Thereby, metal powder is applied in a thin layer onto a build platform and melted locally track-by-track and layer-by-layer using a laser beam. The resulting microstructure is characterized by periodic melt traces, melt pools, elongated grains and a highly refined intragranular cellular structure caused by the high cooling rate during the selective laser melting process [10–14].

This study focuses on selective laser melted 316 L stainless steel. Its corrosion resistance, high ductility, high strength and biocompatibility makes it suitable for medical applications, aerospace and automotive. Due to complex thermal history, the mechanical properties of selective laser melted 316 L components deviate considerably from conventional 316 L. In previous work, selective laser melted 316 L has shown increased yield strength $R_{p0.2}$, ultimate tensile strength R_m combined with decreased ductility, high anisotropy compared to conventional-processed 316 L, as well as a large variance in the range of strength and elongation at break values [15, 16, 11, 10, 4, 5, 17].

Depending on the specimen orientation to build direction, various thermal histories occur within the component resulting in increased mechanical anisotropy of selective laser melted 316 L [18]. In the following, specimen orientation is always related to build direction. There are several studies concerning the influence of specimen orientation on the mechanical properties of as-built selective laser melted 316 L in literature, mostly focusing on specimen orientation of 0° and 90° [17, 19, 5]. A specimen orientation of 90° has shown increased yield strength $R_{p0.2}$ and tensile strength R_m combined with lower ductility compared to a specimen orientation of 0° [10, 20, 17]. The common explanation for this phenomenon is the alignment of deposited layers with respect to loading axis. Loads perpendicular to the boundary layers (specimen orientation 0°) are associated with earlier yielding and

reduced strength whereas loads parallel to the layer boundaries (specimen orientation 90°) are associated with higher tensile strength compared to loads perpendicular to the layers [4, 13]. Results regarding elongation at break A show broad variance in literature with some studies indicating increased elongation at break A for specimen orientation of 0° compared to specimen orientation 90° whereas other studies indicate the exact opposite trend [4, 10, 11, 13, 17, 20]. To date, there are only a few studies concerning the mechanical properties between the two extremes (specimen orientation of 0° and 90°) [4, 17, 20]. In the most comprehensive studies tensile specimens with specimen orientations of 0°, 15°, 45°, 75° and 90° and 0°, 30°, 45°, and 90°, respectively, were investigated [4, 20]. In both studies, an increase in yield strength $R_{p0.2}$ and tensile strength R_m was observed from a specimen orientation of 0° to 90°, with the highest values occurring for a specimen orientation of 45°.

Previous studies in literature have shown that the microstructure and thus mechanical properties and anisotropy of selective laser melted 316 L strongly depends on the specimen orientation to build direction, heat treatment and process parameters (i.e. laser power) [11–14, 21–23]. To date, however, little is known about the influence of specimen thickness on the mechanical properties of selective laser melted 316 L, as most of the studies are performed on bulk specimens with unique specimen thickness (> 1 mm) [5, 10, 11, 13, 24]. Due to the build process during selective laser melting, however, the mechanical properties are expected to be dependent on the structural size. This is particularly relevant for lightweight structures or small medical applications (e.g. coronary stents) to ensure sufficient mechanical properties of these thin lattice-like structures.

The present work focuses on the analysis of the influence of specimen thickness on the mechanical properties of selective laser melted tensile specimens made of 316 L under consideration of different specimen orientations. The correlation between specimen thickness and specimen orientation should allow the derivation of first recommendations for an adequate component design of selective laser melted 316 L parts, especially with regard to filigree structures.

2 Experimental procedure

2.1 Specimen fabrication

Gas-atomized 316 L powder with a particle size of D = 15 µm–45 µm (LPW, Rundkorn, United Kingdom) was used in this study. The chemical composition of the austenitic type stainless steel 316 L powder is given, *Table 1*. As the mechanical properties vary with each batch, the tensile specimens were manufactured in one single production batch using a SLM 250 machine (SLM Solutions Group AG, Lübeck, Germany) equipped with a 400 W Yb-fibre-laser. The process parameters are summarized, *Table 2*. The stripe filling scanning pattern with bidirectional scanning direction was used. Tensile specimen contour was reexposed to the laser after each layer to improve surface quality, *Figure 1*c [25].

Table 1. Chemical composition (wt.-%) of the 316 L powder.
Tabelle 1. Chemische Zusammensetzung (Gew.-%) des 316 L Pulvers.

Element (wt.-%)	C	Cr	Cu	Mn	Mo	N	Ni	O_2	P	S	Si	Fe
316 L	0.019	17.8	0.1	1.12	2.32	0.1	12.65	0.02	0.009	0.005	0.64	balance

Table 2. Process parameters of the selective laser melting process.
Tabelle 2. Prozessparameter des selektiven Laserstrahlschmelzens.

Laser power	Scanning velocity	Focus position	Layer thickness	Hatch distance	Rotation per layer
350 W	700 mm/s	0	50 µm	80 µm	83°

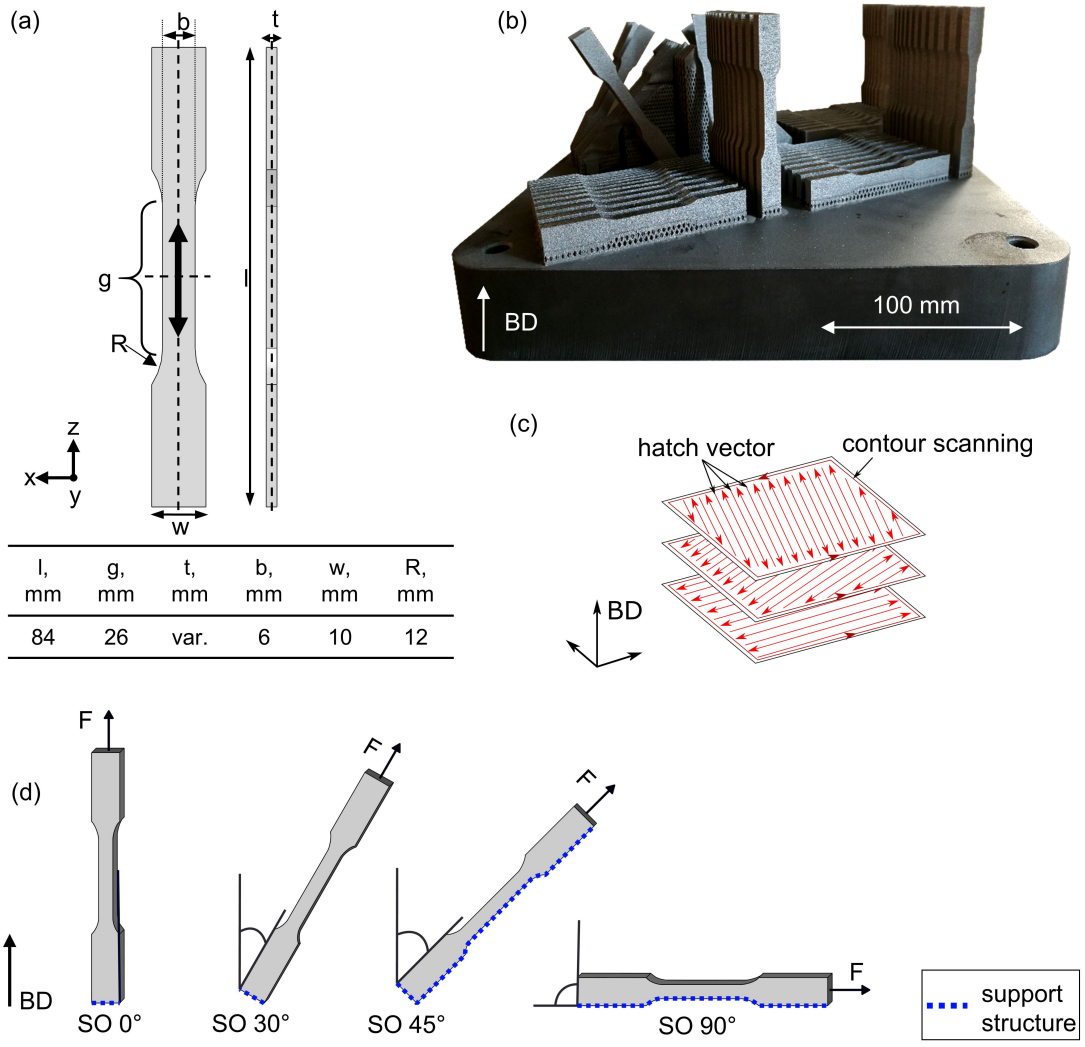

l, mm	g, mm	t, mm	b, mm	w, mm	R, mm
84	26	var.	6	10	12

Figure 1. Tensile specimens used: (a) Illustration of the dimensions of the tensile specimens with the specimens length l, the gauge length g, the width b and the thickness t. The loading direction is indicated by the thick black arrow. (b) As-built 316 L selective laser melted tensile specimens on the build platform. (c) Schematic illustration of the scanning pattern and contour exposure. (d) Schematic representation of the tensile specimen orientation (SO) to build direction (BD) with the loading direction F and the location of the support structure (dotted line).

Bild 1. Untersuchte Zugproben: (a) Darstellung der Abmessungen der Zugproben mit der Länge l, der Messlänge g, der Breite b und der Dicke t. Die Belastungsrichtung ist mit einem dicken schwarzen Pfeil gekennzeichnet. (b) Selektiv lasergeschmolzene Zugproben auf der Bauplattform. (c) Schematische Darstellung des Belichtungsmusters und der Konturbelichtung. (d) Schematische Darstellung der Probenausrichtung (SO) zur Baurichtung (BD) und der Belastungsrichtung F und der Lage der Supportstruktur (gestrichelte Linie).

The main focus of the experimental study has been on the determination of the influence of specimen thickness on the mechanical properties of selective laser melted 316 L, especially with regard to filigree structures (specimen thickness ≤ 2 mm). Tensile specimen geometry was in accordance with the DIN 50125 form E with varying specimen thickness of 0.25 mm, 0.5 mm, 0.75 mm, 1.0 mm, 1.5 mm, and 2.0 mm, Figure 1a [26]. For a more general analysis of the influence of specimen thickness, the study has been extended by the variation of specimen orientation with the specimens being inclined by an angle α of 0°, 30°, 45° and 90° with respect to build direction, respectively, Figure 1c, d. Moreover, for the specimen orientation of 0° and 90° additional tensile specimens with a specimen thickness of 2.5 mm, 3.0 mm, 3.5 mm, 4.5 mm and 5.0 mm were investigated to determine the bulk

material properties, Figure 1b. Of each of the aforementioned sample configurations, 2 tensile samples were prepared and tested. After fabrication, the tensile specimens were cut from the build platform and the supporting structures were removed by grinding. With a sample orientation of 0° and 30°, the support structures were located at the ends of the sample shoulders, with a sample orientation of 90° on the downward-facing longitudinal edge of the sample, and with a sample orientation of 45° both at the end of the sample shoulder and on the downward-facing longitudinal edge of the sample. Apart from the removal of the support structures, the specimens were maintained in their as-built condition and no surface treatment was performed.

2.2 Mechanical testing

Tensile tests were performed at room temperature with a cross-head separation rate of 1 mm/min using an universal testing machine (Hegewald & Peschke Mess- und Prüftechnik GmbH, Nossen Germany). Strain was measured using an extensometer with an initial gauge length of 25 mm. In total 57 tensile specimens were tested in the as-built condition to evaluate the influence of specimen thickness and orientation. The test matrix is given, *Table 3*.

2.3 Metallographic analysis

For metallographic analysis, three cross-sections were taken from the unloaded ends of the tensile specimens remnants with a specimen thickness of 0.5 mm and 2.0 mm for each specimen orientation. For 3D-visualization of the microstructure, these specimens were embedded perpendicular and parallel to build direction in hot mounting resin. The focus of the metallographic analysis has been on the determination of differences in the microstructure (e. g. grain growth, grain shape, melt pool shape) depending on the specimen orientation and on the derivation of a correlation between the microstructure and mechanical properties. After grinding, mirror polishing and etching in hot V2A etchant the microstructural analysis was performed using an

Table 3. Test matrix for the investigation of the mechanical properties of small structures.
Tabelle 3. Testmatrix für die Untersuchung der mechanischen Eigenschaften von kleinen Strukturen.

SO [°] ST [mm]	0	30	45	90	
0.25	0**	2	0**	2	
0.5	2	2	1*	2	
0.75	1*	2	1*	2	
1.0	1*	2	1*	2	
1.5	2	2	1*	2	
2	2	2	1*	2	
2.5	2	–	–	2	
3	2	–	–	2	
3.5	2	–	–	2	
4.0	2	–	–	2	
5.0	2	–	–	2	
Total amount	18	12	5	22	**57**

* one sample was damaged during the removal of the support or during the construction process and was thus not tested. Therefore, only the test results of a single measurement are available.
** two sample were damaged during the removal of the support or during the construction process and was thus not tested. Therefore, no test results are available.

optical light microscope according to standard practice.

3 Results

The evaluation of tensile tests with variable specimen thickness show that the tensile properties of selective laser melted 316 L are not only strongly influenced by specimen orientation as known from literature but also by specimen thickness [4, 5, 11, 19].

3.1 Influence of specimen thickness

In general, an increase in specimen thickness is associated with an increased elongation at break A, yield strength $R_{p0.2}$ and tensile strength R_m for all specimen orientations, *Figure 2*. For a more detailed and quantitative analysis, characteristic values such as yield strength $R_{p0.2}$, tensile strength R_m and elongation at break A, are correlated with specimen thickness for each specimen orientation, *Figure 3*. With increasing specimen thickness, the respective value increases steadily until a saturation

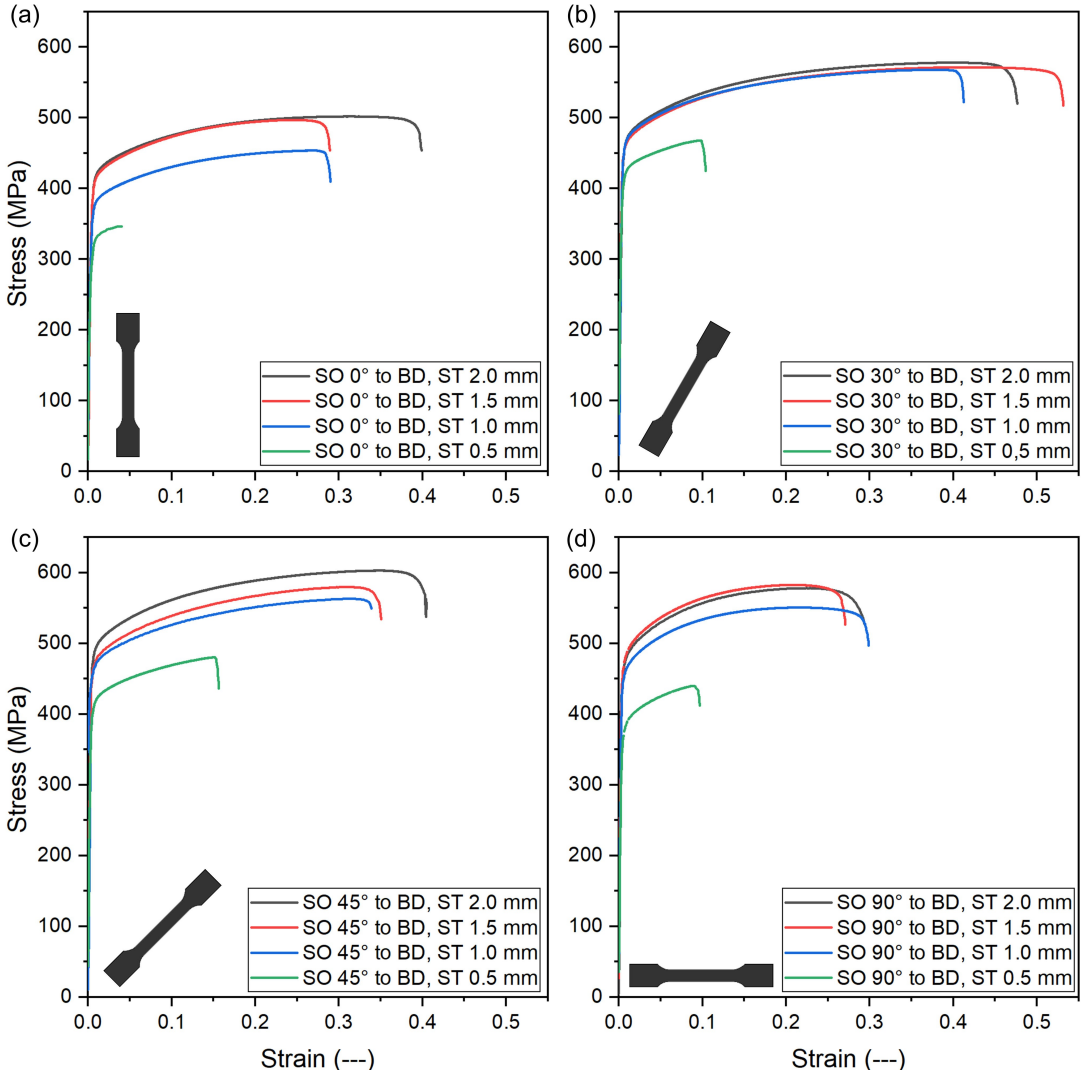

Figure 2. Exemplary representation of the influence of specimen thickness (ST) on the tensile properties of selective laser melted 316 L specimens with various specimen orientation (SO): (a) 0°, (b) 30°, (c) 45° and (d) 90° to build direction (BD).

Bild 2. Exemplarische Darstellung des Einflusses der Probendicke (ST) auf die mechanischen Eigenschaften von selektiv lasergeschmolzener 316 L Probe mit verschiedenen Probenausrichtungen: (a) 0°, (b) 30°, (c) 45° und (d) 90° zur Baurichtung (BD).

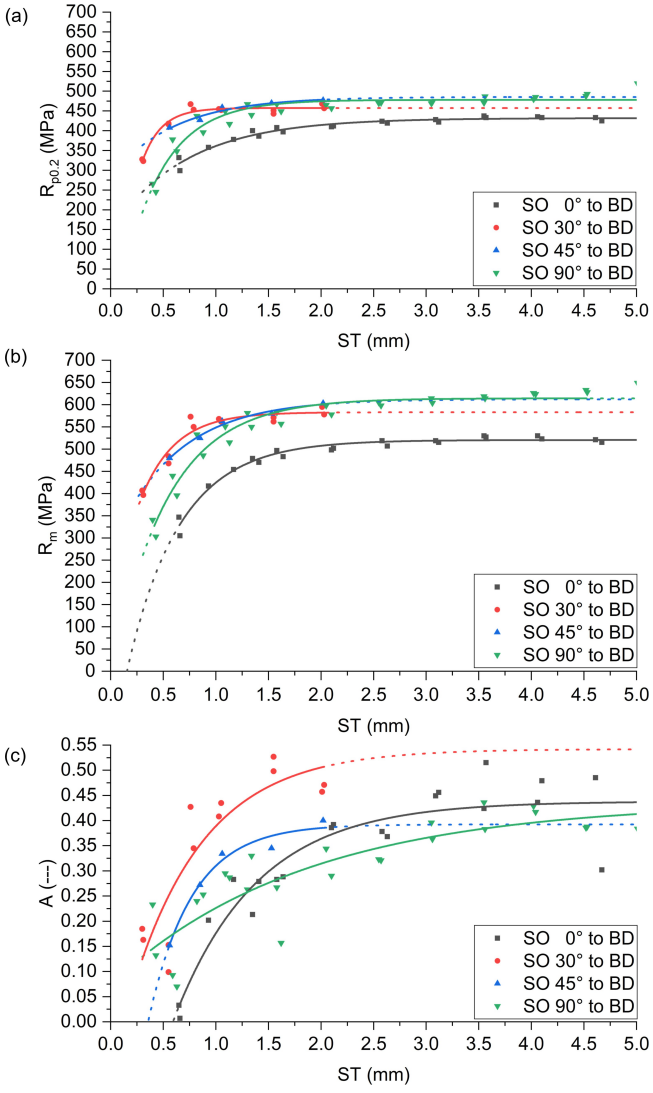

Figure 3. Correlation of specimen thickness (ST) with (a) yield strength $R_{p0.2}$, (b) tensile strength R_m and (c) elongation at break A for various specimen orientation (SO) to build direction (BD).

Bild 3. Korrelation zwischen der Probendicke (ST) und (a) der Dehngrenze $R_{p0.2}$, (b) der Zugfestigkeit R_m und (c) der Bruchdehnung A für verschiedenen Probenausrichtungen (SO) zur Baurichtung (BD).

state for the strength values is reached for a specimen thickness greater than 1.5 mm.

3.2 Influence of specimen orientation

The influence of specimen orientation on the mechanical properties of selective laser melted 316 L is pronounced for thin tensile specimens (< 1.5 mm) and tends to decrease with increasing specimen thickness (> 1.5 mm), Figures 2, 3a, b. For specimen orientations of 30°, 45° and 90°, similar strength is obtained for a specimen thickness higher than 1.5 mm ($R_{p0.2}$: 457 MPa–486 MPa; R_m: 583 MPa–614 MPa), Figures 2, 3a, b. The mechanical properties for a specimen orientation of 0° deviate considerably from the other specimen orientations, with the lowest strengths being observed here. For specimen orientation of 0° yield strength $R_{p0.2}$ is reduced by 9 % and tensile strength R_m by 15 % compared to the values of specimen orientation of 90°. The elongation at break A shows great variation for all specimen orientation with the tendency towards increasing values with increasing specimen thickness. The saturation value, however, is not as pronounced as in the case of the yield and tensile strength. At a specimen thickness of 1.5 mm, elongation at break A varies in the range of approximately 0.2 (specimen orientation 90°) to 0.52 (specimen orientation 30°).

3.3 Phenomenological description

The presented experimental data allows for a derivation of a phenomenological, quantitative relation between material characteristic values and specimen thickness. Based on these findings, subsequent experimental investigations can be reduced to a smaller number of test specimens without neglecting the influence of specimen thickness. Furthermore, this correlation can be used for numerical analyses. Yield strength $R_{p0.2}$, tensile strength R_m as well as elongation at break A can be expressed in terms of an exponential function of specimen thickness (Equation 1). Due to limited data resolution for specimen orientation (0°, 30°, 45° and 90°), the influence of specimen orientation was not explicitly included as a variable in the phenomenological model. However, the influence of specimen orientation was indirectly considered within the phenomenological model by recalibrating the model parameters for each specimen orientation.

$$f(ST) = f_{sat} + C\, e^{k\, ST} \tag{1}$$

ST refers to the specimen thickness. The parameter f_{sat} corresponds to the saturation value of the respective value ($R_{p0.2}$, R_m, A). The parameters *C* and *k* determine the gradient of the exponential

function. More specifically, C, together with f_{sat}, determines the initial value of the function ($f(0\,\text{mm}) = f_{sat} + C$) and k defines the growth rate. The specific function of the respective material parameter ($R_{p0.2}$, R_m, A) is listed together with the fit parameters, the standard error of regression S and the coefficient of determination R^2, *Table 4*. The coefficient of determination R^2 for the phenomenological correlation of the yield strength $R_{p0.2}$ and tensile strength R_m with specimen thickness is in a range from 0.95–0.99 indicating a good fit. Elongation at break A shows greater variance, especially for a specimen orientation of 90°, which in turn results in reduced R^2 values of 0.79–0.92.

3.4 Microstructure analysis

The selective laser melted 316 L shows strongly textured microstructure with columnar grains aligned in build direction, *Figures 4, 5*. The layered microstructure is further characterized by overlapping melt pools, melt traces and elongated grains growing beyond the melt pool boundaries along build direction. A slightly different micro-

Table 4. Phenomenological description of yield strength $R_{p0.2}$, tensile strength R_m and elongation at break A as a function of specimen thickness (ST) for various specimen orientations (SO) including the standard error of the regression S and the coefficient of determination R^2.

Tabelle 4. Phänomenologische Beschreibung der Dehngrenze $R_{p0.2}$, der Zugfestigkeit R_m und der Bruchdehnung A als Funktion der Probendicke (ST) für verschiedene Probenorientierungen (SO) einschließlich des Standardfehlers der Regression S und des Bestimmtheitsmaßes R^2.

$R_{p0.2}$	$R_{p0.2}(ST) = R_{p0.2,sat} + C_{Rp0.2} \cdot ek^{Rp0.2 \cdot ST}$				
SO [°]	$R_{p0.2,sat}$ [MPa]	$C_{Rp0.2}$ [MPa]	$k_{Rp0.2}$	R^2	S [MPa]
0	432.8	−287.2	−1.42	0.9914	7.27
30	457.4	−719.6	−5.54	0.9763	8.93
45	458.6	−203.3	−1.66	0.9539	5.67
90	474.0	−687.1	−2.83	0.9814	17.78
R_m	$R_m(ST) = R_{m,sat} + C_{Rm} \cdot ek^{Rm \cdot ST}$				
SO [°]	$R_{m,sat}$	C_{Rm}	k_{Rm}	R^2	S [MPa]
0	520.5	−708.9	−2.00	0.9922	9.52
30	583.0	−472.1	−3.07	0.9585	15.78
45	612.2	−339.1	−1.67	0.9850	5.31
90	614.4	−635.1	−1.92	0.9859	20.93
A	$A(ST = A_{sat} + C_A \cdot e^{kA} \cdot ST)$				
SO [°]	A_{sat} [MPa]	C_A [MPa]	k_A	R^2	S [MPa]
0	0.435	−0.94	−1.34	0.9268	0.052
30	0.542	−0.64	−1.44	0.8057	0.068
45	0.392	−0.93	−2.42	0.9725	0.001
90	0.452	−0.37	−0.49	0.7936	0.050

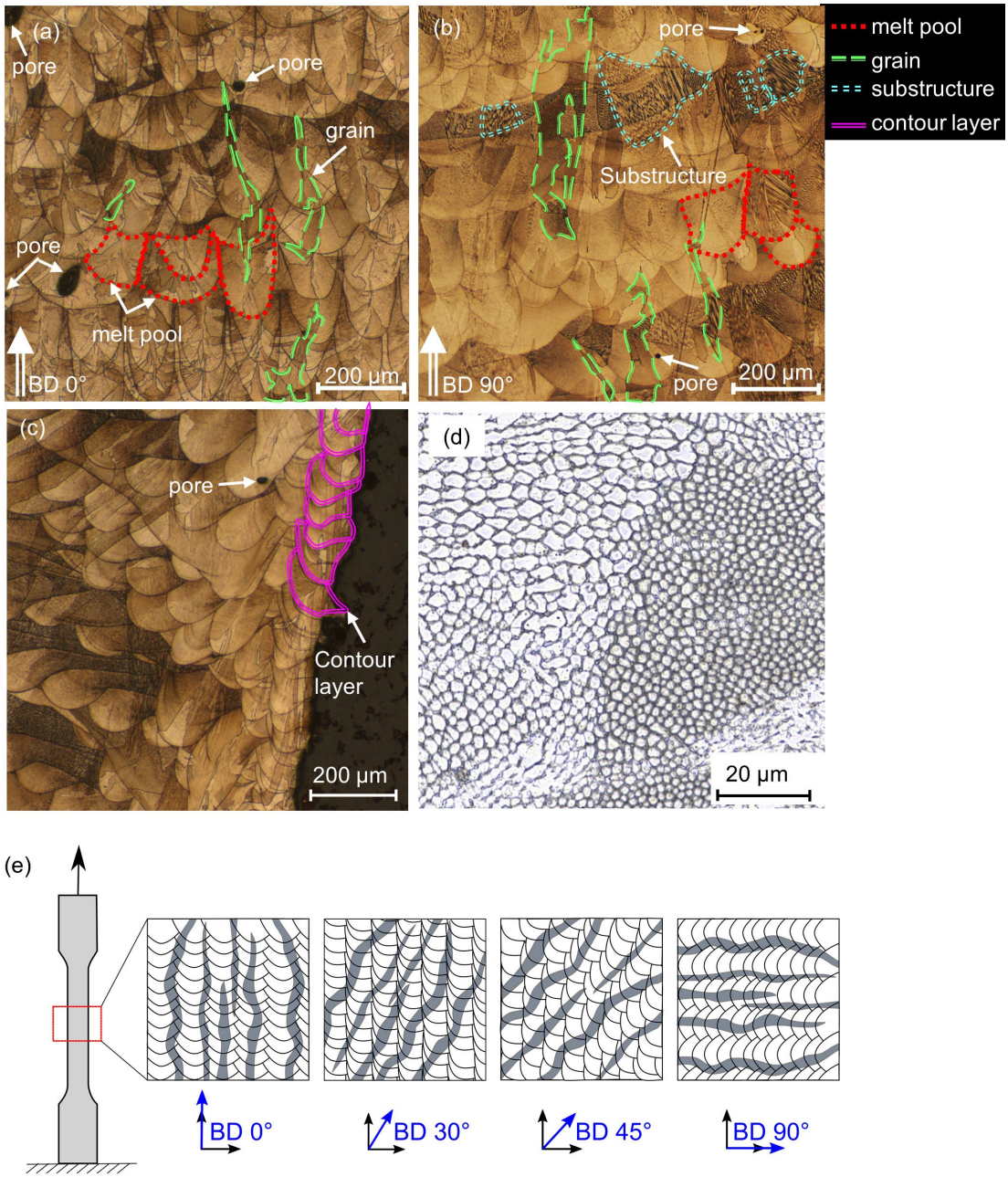

Figure 4. Microstructure of selective laser melted 316 L: Illustration of elongated grains (green), fine substructure (blue), melt pools in the bulk material (red) and the contour exposure areas (pink) on a metallographic section with a specimen orientation of (a) 0°, (b) 90°, (c) 30° highlighting the re-melted melt pools of the contour area, (d) illustration of the fine intragranular substructure and (e) a schematic illustration of the basic microstructure resulting from the various specimen orientations.

Bild 4. Mikrostruktur des selektiv lasergeschmolzenen 316 L: Darstellung der langgestreckten Körner (grün), der feinen Substruktur (blau), des Schmelzbades im Vollmaterial (rot) und des Bereichs der Konturbelichtung (pink) anhand von metallographischen Schliffen der Probenorientierung von a) 0°, (b) 90°, (c) 30° mit Fokus auf des wiederaufgeschmolzenen Schmelzbades des Konturbereichs, (d) Darstellung der feinen intragranularen Substruktur und (e) schematische Darstellung der grundlegenden Mikrostruktur der verschiedenen Probenausrichtungen.

structure with smaller melt pools is observed in the contour exposure area, Figure 4c. In the bulk material, melt pool width is approx. $D_{MP,bulk} = 130\ \mu m$–$150\ \mu m$ and in the contour area $D_{MP,cont} = 90\ \mu m$–$100\ \mu m$. Furthermore, a fine intragranular substructure can be detected, Figure 4b, d.

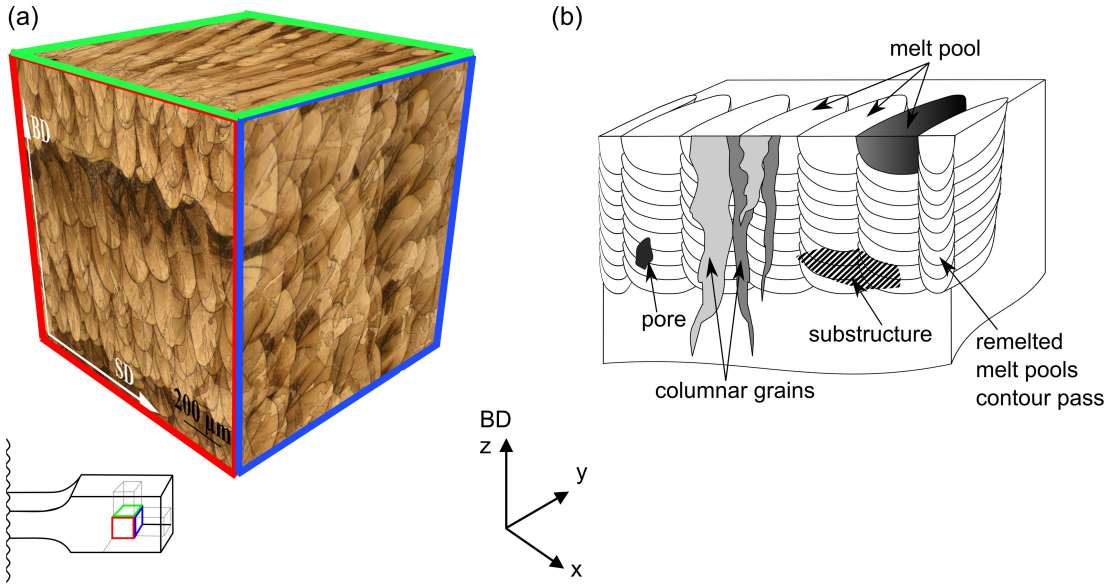

Figure 5. 3-dimensional representation of the microstructure of the selective laser melted 316 L exemplary on a specimen orientation (SO) of (a) 90° to build direction (BD) and (b) a schematic illustration of the basic 3-dimensional microstructure.

Bild 5. 3-dimensionale Darstellung der Mikrostruktur des selektiv lasergeschmolzenen 316 L: a) exemplarisch an einer Probe mit der Orientierung von 90° zur Baurichtung und b) eine schematische Darstellung der grundlegenden 3-dimensionalen Mikrostruktur.

4 Discussion

4.1 Microstructure

The periodically well-aligned arc-shaped melt pool structure can be attributed to the Gaussian energy distribution of the laser and repeated partially track-by-track and layer-by-layer remelting by the laser. The elongated columnar grains spreading across the melt pool boundaries indicate epitaxial growth from remelted areas. Grain growth direction thereby tends to follow the maximum thermal gradient towards the melt pool center [13, 4].

The fine intragranular substructure is reported to be δ-ferrite [27, 19]. The role of the substructure has not been clarified yet. According to other studies, the substructure consists of δ-ferrite, which has a higher chromium and molybdenum content than the austenitic matrix. Due to its higher strength compared to austenite, the finely distributed δ- ferrite increases the overall strength. The specific morphology of the δ-ferrite could be different for vertically and horizontally aligned specimens, as the cooling conditions might vary significantly. The determination of the exact distribution of δ-ferrite of the different specimens was not part of this work, but should be a part of subsequent research. The strength-increasing effect of δ-ferrite can be seen in particular in heat treatments, which dissolve the δ-ferrite but leave the grain structure of the austenite unaffected [28, 23]. This reduces the strength to values similar to those of conventionally processed 316 L [28].

4.2 Specimen thickness dependency

The results indicate that thinner structures exhibit consistently lower strength and ductility which is consistent with the findings on round tensile specimens [29]. It is assumed that the saturation of the specific material properties are achieved for a specimen diameter greater than 3 mm–5 mm [29–31]. In this study, the results for flat tensile specimens indicate that the saturation value of the material properties can be achieved for a specimen thickness greater than approximately 1.5 mm.

The overall reduction in strength and ductility for thinner specimen thickness might be attributed to the larger surface to volume ratio resulting in an increased susceptibility to local imperfections, such as pores or incompletely fused areas, or to notch effects due to the layered structure resulting from the selective laser melting process [29, 31]. Moreover,

larger specimen thickness indicate more material for plastic flow and thus for dislocation movement resulting in an increased elongation at break A [31].

The reduced strength for small specimen thickness could further be related to a deviation in the determination of specimen cross-sectional area from a real value. Due to partially molten powder particles attached to the specimens as well as potential defects (e. g. pores, unfused material), the specimen cross-sectional area might be assumed to be too large compared to the real specimen cross-section, *Figure 6*.

Pores with sectional diameter D_{pore} of approx. 60 µm–80 µm were determined from the metallographic section of specimen with a thickness of 0.5 mm. With a maximum powder grain diameter $D_{grain,max}$ of 45 µm and a pore size D_{pore} of 80 µm, this can lead to an maximum estimated measurement error of up to 0.17 mm ($2 \cdot D_{grain} + D_{pore}$). This measurement error would thus lead to an overestimation of the cross-sectional area of 70 % for a specimen thickness of 0.5 mm and an overestimation of 9 % for a specimen thickness of 2 mm. To consider this effect, the width used to determine the cross-sectional area of the specimens for stress calculation was reduced by 90 µm. This corresponds, e. g. to the adhesion of two maximum large powder particles ($2 \cdot D_{grain,max}$) or the existence of a representative pore with a diameter of D_{pore} 70 µm and a minimum adhesive powder grain diameter $D_{grain,min}$ of 10 µm. After correcting the cross-sectional areas to account for adhering powder grains and defects, saturation of the strength values is already achieved at smaller specimen thickness (>1 mm). However, there is a distinct drop of the tensile strength especially in the area of small specimen thickness (≤ 1 mm), Figure 6a, b.

Moreover, the chosen contour exposure might also induce specimen thickness dependent material properties. After the completion of each layer, the contour of the tensile specimens is remelted with the laser to improve surface quality. This results in different heat input and cooling conditions compared to the primary manufacturing process, as the bulk material has already cooled down partially. However, these effects are very complex and depend both on the process parameters and the specimen geometry/thickness due to different cooling rates between thin and thicker specimens. In the

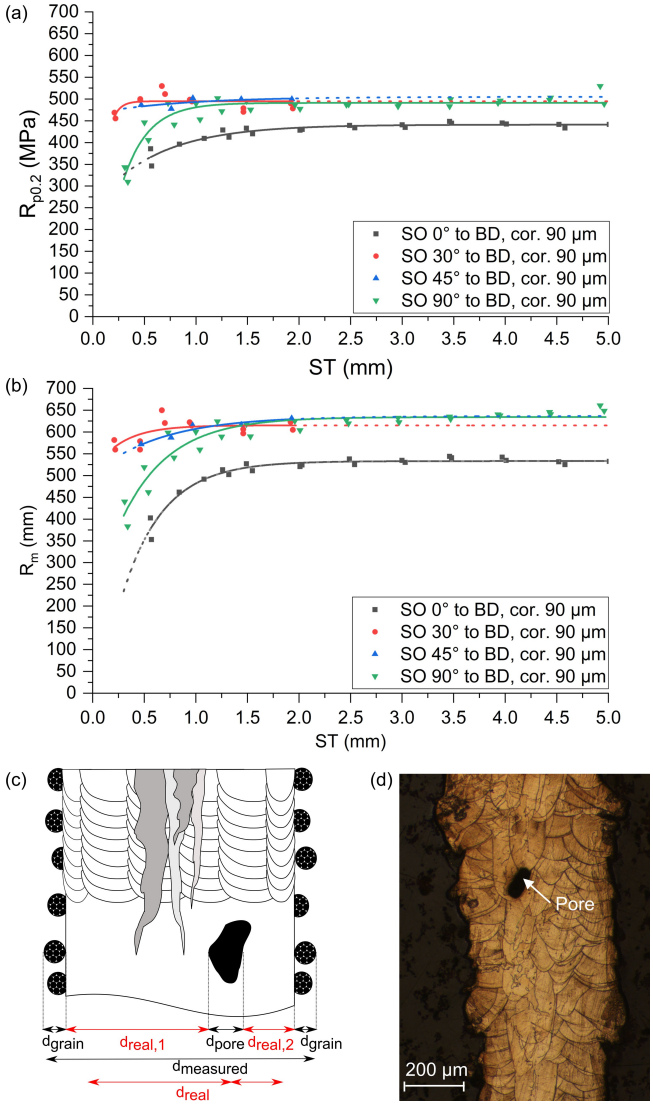

Figure 6. Correlation of the strength values and specimen thickness after surface area measurement correction: (a) Yield strength $R_{p0.2}$ and (b) tensile strength R_m with measurement correction by reducing the specimen thickness by 0.09 mm. (c) Schematic illustration of the potential cross-sectional deviations due to pores and adhering powder particles. (d) Exemplary microstructure of a specimen orientation of 0° with a specimen thickness of 0.5 mm illustrating pores and surface roughness.

Bild 6. Korrelation der mittleren Festigkeitswerte und der Probendicke nach Korrektur der gemessenen Probenquerschnittsfläche: (a) Dehngrenze $R_{p0.2}$ und (b) Zugfestigkeit R_m unter Berücksichtigung der Querschnittflächenkorrektur durch eine Verringerung der Probendicke um 0,09 mm. (c) Schematische Darstellung der potenziellen Querschnittsabweichungen aufgrund von Poren und anhaftenden Pulverpartikeln. (d) Beispielhafte Mikrostruktur einer Probenorientierung von 0° mit einer Probendicke von 0,5 mm zur Veranschaulichung von Poren und Oberflächenrauigkeit.

area of the component near-surface layer, a different microstructure is formed which is characterized by e. g. smaller melt pool widths. Therefore, material properties deviating from those of bulk material are to be expected in the component near-surface area. However, explicit investigations concerning this assumption were not part of this investigation. So far, contour exposure has mainly been used to improve surface quality. However, investigations into the influence of contour exposure on the mechanical properties of AM components have not been performed yet. The influence of contour exposure on the mechanical properties of additively manufactured components considering specimen geometry and the process parameters should therefore be part of subsequent research.

4.3 Specimen orientation dependency

In this study, explicit consideration of the specimen orientation on the characteristic values is omitted within the phenomenological description (Equation 1) due to limited data resolution (only four different specimen orientations tested). However, there is a general tendency of the influence of specimen orientation on the mechanical properties of selective laser melted 316 L. The tensile test results indicate that specimen orientation dependency is particular pronounced for small structures (specimen thickness < 1.5 mm). With larger specimen thickness, specimen orientation dependency is hardly noticeable for specimen orientations of 30°, 45° and 90°, whereas there is a clear deviation in strength to the specimen orientation of 0°. Specimen orientation of 0° shows the lowest strength values for all specimen thicknesses. To date, this phenomenon has not yet been fully clarified in the literature [4]. However, there are some explanatory approaches which should be discussed in the following.

The most frequently cited reason for the different strength and ductility between vertically and horizontally aligned specimens is the strong anisotropy caused by the layer-by-layer manufacturing process of selective laser melting and the resulting elongated grains [32, 13]. The common explanation for this phenomenon is the alignment of deposited layers with respect to loading axis. Loads perpendicular to the melt pool layers (specimen orientation 0°) are associated with earlier yielding and reduced strength, whereas loads parallel to the layer boundaries (specimen orientation 90°) are associated with higher tensile strength [13]. Ductility of selective laser melted 316 L can be traced back to slipping movements between the grain and melt pool boundaries, whereby slipping occurs preferentially at the melt pool boundaries due to weaker bonding forces compared to the grain boundaries [17]. The higher elongation at break for specimen orientation of 0° than for 90° can be explained by higher deformation resistance due to loading direction parallel to elongated grains and thus larger grain boundaries acting as barriers to dislocations motions. Anisotropic ductility might be related to the number of melt pool boundary slipping surfaces in the load direction [17]. Sliding occurs preferably between adjacent melt pools ('track-track') at a load parallel to the boundary layers (specimen orientation 90°), whereby the distance between these adjacent melt pools corresponds to hatch-spacing of 80 µm [17]. With a load perpendicular to the boundary layers (specimen orientation 0°), slipping occurs both between the adjacent melt pools ('track-track') and between the melt pool layers ('layer-layers'). The distance between the melt pool layers corresponds to the layer thickness of 50 µm and thus to about 60 % of the hatch distance. The increased ductility for specimen orientation 0° can thus be attributed to the increased number of sliding surfaces compared to specimen orientation 90° [17]. Furthermore, with the aligned elongated grains in build direction, the texture of selective laser melted materials along build direction is comparable with rolling textures. Depending on the loading direction, the elongated grains gives the structure a fine- or coarse-grained appearance. In the build or rolling direction, the microstructure appears most fine-grained leading to anisotropic mechanical properties [33].

In literature, differences in strengths are partly attributed to residual stresses resulting from different volume energy and cooling conditions [34, 18]. Heat induced during the additive manufacturing process must be dissipated via the already solidified parts material, the support structure and the powder. Due to significantly higher heat transport capability, considerably more heat can be dissipated via the support structure than via the powder. This means that fully supported specimens can cool

down faster after exposure than specimens with a minimum of support. Due to varying cooling rates, the microstructure is formed differently, e. g. by an increased formation of δ-ferrite. If this effect was mainly responsible for the differences in mechanical properties, it would be expected that specimens with a specimen orientation of 0° and 30° would have similar properties since these two orientations are only supported on the specimen shoulders and thus exhibiting similar cooling conditions. However, this could not be found in this study as the mechanical properties of the specimen orientation of 30° are similar to those of specimen orientation of 45° and 90° even though these are fully supported on the build platform. Since there has been a considerable difference in the mechanical properties of specimen orientation of 0° and 30°, it is to be assumed that the different mechanical properties observed in this study result from additional contributing factors, e. g. orientation of grains and grain boundaries with respect to loading directions, besides the different cooling conditions.

Defects are usually considered to reduce ductility and strength. These include bonding defects between the layers, pores, melt pool boundaries or unmelted powder particles. This study indicates that defects might lead to deviations between the real cross-section and the measured cross-section. This leads to the calculation of lower strength values, but can be corrected if the representative pore size is known. Especially in case of thin specimens, voids might contribute to earlier failure due to stress peaks near the voids [28].

In summary, there are a large number of phenomena and process specific parameters which influence the specimen orientation-dependent mechanical properties. Due to different tendencies in related studies (e. g. regarding the increased elongation at break for specimen orientation 0°, e. g. [13, 17, 4, 5, 32]) the specimen orientation dependent ductility in additive manufacturing has not yet been fully understood [4]. Therefore further in-depth investigations, e. g. with regard to the influence of δ-ferrite, imperfection such as unfused areas or pores, and surface quality are required.

4.4 Design recommendation for additive manufactured structures

The strongly pronounced texture and the associated anisotropy of the mechanical properties of selective laser melted 316 L should be considered for the design of small additive manufactured components. The results of this work can be used for the derivation of design recommendations. It is recommended that components with critical stress/strain conditions are aligned to build direction in such a way that the required mechanical properties are achieved in the specific location. Loads vertical (specimen orientation 90°) or parallel (specimen orientation 0° to build direction) should be avoided wherever possible, as either low strength (specimen orientation 0°) or low ductility (specimen orientation 90°) is to be expected here. Furthermore, the impact of the size effect on mechanical properties must also be considered when designing the component. Components with a specimen thickness less than 2 mm must be designed either with the characteristic values obtained from specimens with corresponding dimensions/thicknesses or with the aid of a corrected bulk characteristic values'. As the correction is derived from uniaxial tensile tests it can only be subjected to tensile loaded components. Yield strength $R_{p0.2}$ can be extrapolated up to a specimen thickness of 0.5 mm by considering a representative error/pore. However, the defect diameter determined here is not transferable to other build conditions/parameters, since, e. g. component porosity is influenced by laser power. The correction factor must therefore always be determined individually. The consideration of the size effect in additive manufacturing is particularly important in case of thin-walled and weight-optimized components.

4.5 Limitations

Since only two samples per sample thickness and orientation were tested, the data obtained in this study are not sufficient to make statistically reliable statements. The presented results show that the mechanical properties of additively manufactured tensile specimens made of 316 L are influenced by the specimen thickness. Therefore, to substantiate these results, further investigations should be carried out

with a higher number of samples. This will allow the verification of the results of this first study and a more reliable design of small additively manufactured components.

5 Conclusion

Specimen thickness and orientation have a significant effects on the mechanical properties of selective laser melted 316 L. Therefore, only specimens with the same specimen orientation and thickness can be compared and used for component design considerations. It could be shown that the strength values increase with increasing specimen thickness and that a saturation value is reached from a specimen thickness greater than 2 mm. For filigree structures, their specific material properties structures have to be determined or adapted e. g. by using a correction factor which allows for the consideration of pores and adhering powder grains within the measured volume. Specimen orientation dependent strength is particularly pronounced at smaller specimen thicknesses. In the saturation area, however, approximately similar values are achieved for specimen orientation of 30°, 45° and 90°, whereas the lowest strength is achieved for specimen orientation of 0°. For the determination of material properties of selective laser melted 316 L with different process parameters, it might therefore be sufficient to test tensile specimens with a specimen orientation of 0° and 90°, since the properties of the inclined specimens correspond approximately to those of the specimen orientation of 90° specimens. Furthermore concerning component design, loads vertical (specimen orientation 90°) or parallel (specimen orientation 0°) to build direction, should be avoided wherever possible, as either low strength or low ductility is to be expected.

Acknowledgements

This work was supported by Bayerische Forschungsstiftung ["NewGen-Stent": grant number AZ-1221-16]. This work is further supported by the Bavarian Academic Forum (BayWISS) Doctoral Consortium Health Research and the State Conference for Women and Equal Opportunity Officers at Bavarian Universities (LaKoF). Open access funding enabled and organized by Projekt DEAL

6 References

[1] W. Gao, Y. Zhang, D. Ramanujan, K. Ramani, Y. Chen, C.B. Williams, C.C. Wang, Y. C. Shin, S. Zhang, P.D. Zavattieri, *Comput. Aided Des* **2015**, *69*, 65.
[2] J. Holmström, J. Partanen, J. Tuomi, M. Walter, *J. Manuf. Technol. Manag.* **2010**, *21*, 687.
[3] J.J.S. Dilip, S. Zhang, C. Teng, K. Zeng, C. Robinson, D. Pal, B. Stucker, *Progress in Additive Manufacturing* **2017**, *2*, 157.
[4] L. Hitzler, J. Hirsch, B. Heine, M. Merkel, W. Hall, A. Ochsner, *Materials* **2017**, *10*, 1136.
[5] E. Liverani, S. Toschi, L. Ceschini, A. Fortunato, *J. Mater. Process. Technol.* **2017**, *249*, 255.
[6] J. Kranz, D. Herzog, C. Emmelmann, *J. Laser Appl.* **2014**, *27*, 14001.
[7] P. Pradel, Z. Zhu, R. Bibb, J. Moultrie, *J. Eng. Des.* **2018**, *29*, 165.
[8] C.C. Seepersa, J. Allison, S. Conner, presented at the *21st International Conference on Engineering Design*, Glasgow, Scotland, August 21–25, **2017**, *5*, 309.
[9] B. Leutenecker-Twelsiek, C. Klahn, M. Meboldt, *Procedia CIRP* **2016**, *50*, 408.
[10] C.M. Davies, R. Zhou, O. Withnell, R. Williams, T. Ronneberg, P.A. Hooper, *Procedia Struct. Integrity*, **2018**, *13*, 1384.
[11] J. Suryawanshi, K.G. Prashanth, U. Ramamurty, *Mater. Sci. Eng. A.* **2017**, *696*, 113.
[12] D. Wang, C. Song, Y. Yang, Y. Bai, *Mater. Des.* **2016**, *100*, 291.
[13] R. Casati, J. Lemke, M. Vedani, *J. Mater. Sci. Technol.* **2016**, *32*, 738.
[14] Y. Zhong, L. Liu, S. Wikman, D. Cui, Z. Shen, *J. Nucl. Mater.* **2016**, *470*, 170.
[15] P. Hanzl, M. Zetek, T. Baksa, T. Kroupa, *Procedia Eng.* **2015**, *100*, 1405.
[16] W.E. Frazier, *JMEP* **2014**, *23*, 1917.
[17] W. Shifeng, L. Shuai, W. Qingsong, C. Yan, Z. Sheng, S. Yusheng, *J. Mater. Process. Technol.* **2014**, *214*, 2660.

[18] M.S.I.N. Kamariah, W.S.W. Harun, N.Z. Khalil, F. Ahmad, M.H. Ismail, S. Sharif, *IOP Conf. Ser. Mater. Sci. Eng.* **2017**, *257*, 012021.
[19] T. Kurzynowski, K. Gruber, W. Stopyra, B. Kúznicka, E. Chlebus, *Mater. Sci. Eng. A.* **2018**, *718*, 64.
[20] I. Tolosa, F. Garciand'ıa, F. Zubiri, F. Zapirain, A. Esnaola, *Int. J. Adv. Manuf. Tech.* **2010**, *51*, 639.
[21] O. Fergani, A. Bratli Wold, F. Berto, V. Brotan, M. Bambach, *Fatigue Fract. Eng. M.* **2018**, *41*, 1102.
[22] A. Riemer, S. Leuders, M. Thöne, H.A. Richard, T. Tröster, T. Niendorf, *Eng. Fract. Mech.* **2014**, *120*, 15.
[23] K. Saeidi, X. Gao, F. Lofaj, L. Kvetková, Z.J. Shen, *J. Alloy Compd.* **2015**, *633*, 463.
[24] A. Mertens, S. Reginster, H. Paydas, Q. Contrepois, T. Dormal, O. Lemaire, J. Lecomte-Beckers, *Powder Metall.* **2014**, *57*, 184.
[25] E. Yasa, J.-P. Kruth, *Procedia Eng.* **2011**, *19*, 389.
[26] DIN Deutsches Institut für Normung e. V., *Prüfung metallischer werkstoffe –zugproben*, Germany, **2016**.
[27] A. Yadollahi, N. Shamsaei, S.M. Thompson, D.W. Seely, *Mater. Sci. Eng. A.* **2015**, *644*, 171.
[28] M.L. Montero Sistiaga, S. Nardone, C. Hautfenne, J. Van Humbeeck, presented at *the 27th Annual International Solid Freeform Fabrication Symposium- An Additive Manufacturing Conference*, Austin, Texas, August 08–10, **2016**, pp. 558.
[29] G. Reinhart, S. Teufelhart, F. Riss, *Phys. Procedia* **2012**, *39*, 471.
[30] L. Hitzler, M. Merkel, W. Hall, A. Öchsner, *Adv. Eng. Mater.* **2018**, *20*, 1700658.
[31] S.J. Merkt, *Ph.D. Thesis*, RWTH Aachen, Germany, **2015**.
[32] L. Ladani, J. Razmi, S. Farhan Choudhury , *J. Eng. Mater.-T. ASME* **2014**, *136*, 96.
[33] M. Garibaldi, I. Ashcroft, M. Simonelli, R. Hague, *Acta Mater.* **2016**, *110*, 207.
[34] H. Meier, C. Haberland, *Materialwiss. Werkst.* **2008**, *39*, 665.

Received in final form: August 7th 2020

